Near-simultaneous polarization and spectral optical measurements of geosynchronous satellites

L. A. Zimmerman, S. S. Chun, M. F. Pirozzoli, M. K. Plummer, F. K. Chun,
Dept. of Physics, United States Air Force Academy, USAF Academy, CO 80840
D. M. Strong
Strong EO Imaging, Inc., Colorado Springs, CO 80908

1. ABSTRACT

The Department of Physics at the United States Air Force Academy has been developing new methods of characterizing space objects using unresolved optical imagery. In the past, we have observed geosynchronous (GEO) communication satellites either photometrically, spectrally, or through polarized filters, but we have never observed these satellites in a near simultaneous fashion through more than one of those optical modes. For this research, we use two modes of analysis, polarimetry and spectroscopy, to characterize several GEO communications satellites which cannot be resolved with ground-based optical imagery due to their size and distance. Our observations are made using a 16-inch telescope outfitted with a 9-position filter wheel populated with broadband photometric filters (Johnson-Cousins B, V, and R; and a blue-blocking exoplanet filter), linear polarization filters (0 degrees, 45 degrees, 90 degrees, 135 degrees), and a 100 lines per millimeter diffraction grating. The spectral measurement is made using the diffraction grating, while the polarization measurement is made using the polarization filters. This research compares the spectra and polarization signatures collected from solar reflectance off of known GEO communication satellites during the Spring 2020 equinox. These observations were made both during a glint and outside of a glint period, and show very different signatures which presumably are due to reflectance from different spacecraft surfaces. More detailed analysis and correlation of a satellite's spectral and polarization signatures are clearly warranted, and in the future should also be related to physical properties of the satellites.

2. INTRODUCTION

Space object characterization is fundamental to space domain awareness, a key capability of the United States Space Force. The Space Force mission is to protect US interests in space, to include communications and intelligence satellites [1]. The space environment contains thousands of resident space objects that are difficult to resolve and characterize on the basis of optical imagery. Most satellites will appear as an unresolved point source in optical images due to the spacecraft's size and the observation distance. As a result, it is necessary to develop new methods to characterize satellite imagery from point source images.

In the past, researchers have employed a variety of methods to characterize unresolved satellite imagery. Satellite shape has been determined using information from a satellite's light curve [2], and satellite surface materials have been studied using multi-band optical observation techniques [3]. Spectral research has concluded that satellite spectra shift toward the red side of the spectrum when exposed to the space environment [4]. There has also been spectral research conducted in attempts to discern surface materials of geosynchronous earth orbit (GEO) satellites [5]. Other satellite features such as orientation have been studied by comparing the spectra of satellites to the spectrum of the Sun [6]. Polarimetry analysis conducted on satellites demonstrated that polarization signatures can characterize and distinguish different types of communication satellites in GEO [7]. Our research will utilize a new polarization- and spectroscopy-based sensing modality for the US Air Force Academy's 16-inch telescope. We will compare results from these two sensing modalities in order to ascertain features common in both optical measurements. This paper will discuss the theory and fundamental science behind our process, methods and procedures, data results, and conclusions and future work.

Copyright © 2020 Advanced Maui Optical and Space Surveillance Technologies Conference (AMOS) – www.amostech.com

3. THEORY

This research project measures the polarimetry and spectroscopy signatures of GEO communication satellites to identify optical features common across both modalities. The polarimetry signatures observed were created by unpolarized light from the Sun reflecting off the observed satellites. When unpolarized light is incident at Brewster's angle, the reflected light is completely polarized parallel to the reflecting surface; likewise, when light is incident upon a surface at any other angle, there will be a varying amount of polarization. As a result, by examining the resulting polarization of light reflected off a material, one can deduce information about satellite properties such as surface material and orientation. The satellite's surface material may indicate the vehicle's subsystems and capabilities, because different materials are used to facilitate various satellite functions. We observe light reflected off a satellite's solar panels and body, whose polarization properties depend on the indices of refraction of the satellite components.

The linear polarization of light can be fully characterized by the first three Stokes parameters:

$$\vec{S} = [S_0\ S_1\ S_2\ ], \tag{1}$$

where S_0 is the total intensity of the light, S_1 is the preference of light polarized in the 0° versus the 90° direction ($S_1 = I_{0^\circ} - I_{90^\circ}$), and S_2 is the preference of light polarized in the 45° versus the 135° direction ($S_2 = I_{45^\circ} - I_{135^\circ}$). The fourth Stokes parameter, S_3, describes how much of the light is polarized in a right-handed versus left-handed circular direction. S_3 is not considered in this analysis.

When light enters a telescope or any optical device, the light's polarization characteristics will be modified due to reflection off the primary and secondary mirrors and transmission through the corrector optics and other optical filters and lens. The camera system measures the intensity of light exiting the telescope, but in order to determine the polarization signature of a satellite incident to the telescope, the measured intensities must be converted to Stokes parameters. To accomplish this, a matrix conversion, W, is utilized. The W matrix accounts for the polarization effects of the telescope optics upon the measured intensities. This assumes that the camera is not polarization sensitive and itself does not produce any polarization effects.

$$\vec{S}_{in} = W[I_0\ I_{45}\ I_{90}\ I_{135}\ ] \tag{2}$$

The W matrix converts the measured intensities to the incident Stokes parameters, estimating the polarization signature reflected from the satellite.

To determine the W matrix for the telescope, we use Malus' law, which relates the outgoing light intensity from a polarization filter to the orientation angle of a polarized film:

$$I(\theta) = I(0)cos^2(\theta), \tag{3}$$

where θ represents the angle between the incident light's polarization and the polarization film or polarizer. This calibration process entails the rotation of a polarization film at 10° increments. Previous work determined that light attenuation for each polarization filter (0°, 45°, 90°, 135°) followed Malus' law and confirmed that the system was calibrated properly [8].

Copyright © 2020 Advanced Maui Optical and Space Surveillance Technologies Conference (AMOS) – www.amostech.com

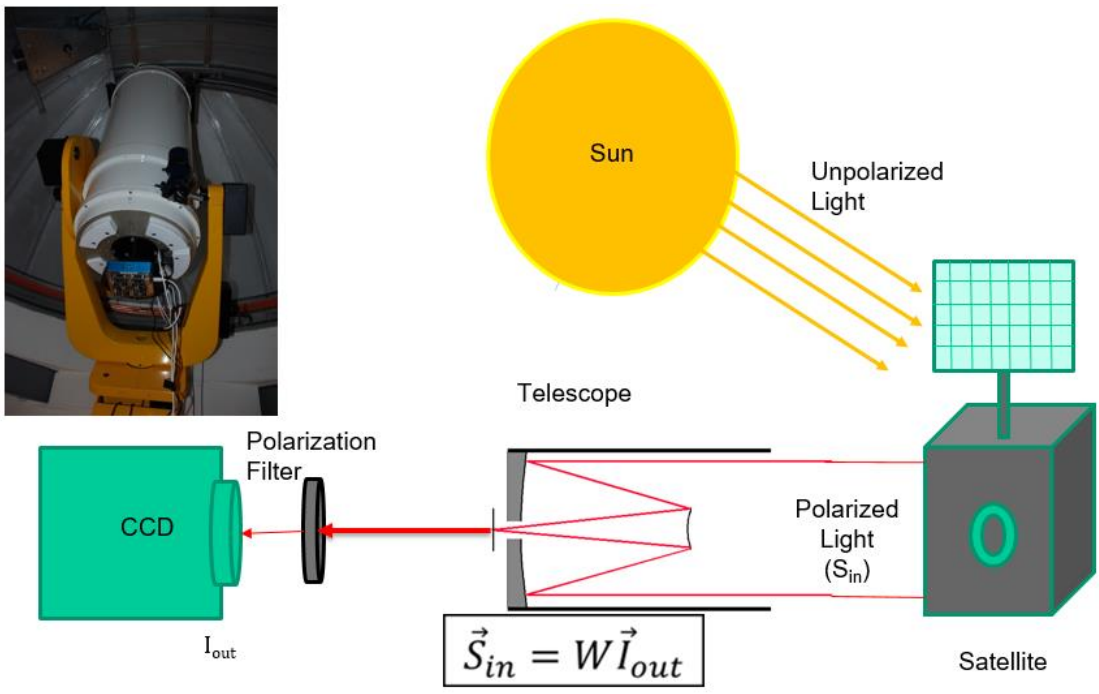

Fig. 1. Schematic of polarimetry data collection. Unpolarized light from the Sun is polarized upon reflection off the satellite. This polarized light is collected by the telescope and then the CCD. The Stokes parameters of the original polarized light can be obtained from telescope data using the *W* matrix.

Fig. 1 illustrates how light, polarized during reflection off of a satellite, travels through the telescope and polarization filter to be collected by the charge-coupled device (CCD) camera sensor. The filter wheel also included a 100-line-per-millimeter diffraction grating that provides low-resolution spectral measurements. Diffraction gratings disperse incident light into components by wavelength, creating a spectrum which spatially corresponds to the wavelength of incident light. The use of slitless rather than slitted spectroscopy allows us to measure the spectra of multiple satellites in the same frame and does not require the satellite to be kept within a narrow slit, as with conventional spectrometers [9]. Fig. 2 shows the experimental setup in which light is reflected from the primary and secondary mirrors and then passes through the grating.

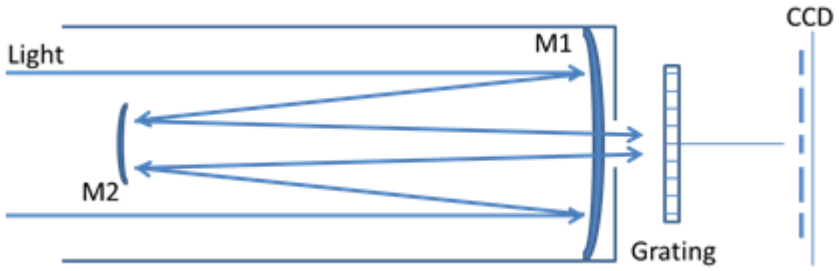

Fig. 2. Illustration of telescope setup, diffraction grating, and CCD. Light enters the telescope, reflects off the primary (M1) and secondary (M2) mirrors, and passes through the diffraction grating before being detected by the CCD.

Copyright © 2020 Advanced Maui Optical and Space Surveillance Technologies Conference (AMOS) – www.amostech.com

4. METHODS AND PROCEDURES

All satellite images are captured by the USAFA DFM f/8.2 16-inch telescope. An Andor Alta U47 1024×1024 pixel CCD camera and a 9-position filter wheel are attached to the telescope resulting in a field of view of 13 arc minutes per camera axis. The filter wheel contains polarization filters oriented at 0°, 45°, 90°, and 135° relative to the vertical axis of the camera's focal plane. To determine incident intensities at each angle, we obtain images by rotating through each filter. We also capture images using the diffraction grating to obtain spectra for each satellite. The orientation of the filter wheel and the orientation of the polarization filters are shown in Fig. 3. Our research used the polarization filters, shown in gray, and the diffraction grating marked 'DG.' Other unused components of the filter wheel are the Johnson-Cousins filters, labeled "B" (blue), "V" (visible), and "R" (red), and a wide-bandwidth filter used for exoplanet research, labeled "Ex".

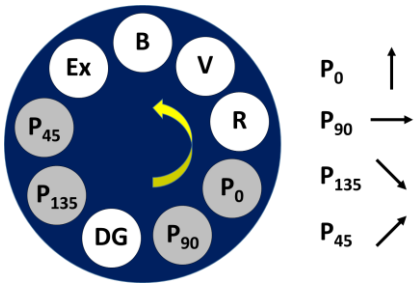

Fig. 3. Filter wheel schematic, showing configuration of the polarization filters and diffraction grating. The arrows to the right show direction of polarization for each filter relative to the vertical axis of the camera's focal plane. The filter wheel rotates counter-clockwise as indicated by the yellow arrow, resulting in the measurement order of P_0, P_{90}, DG, P_{135}, and P_{45}.

Our study focuses on observing operational GEO communication satellites with large solar panels during glint season. Glint season is the time period in which the proper geometry exists to detect the specular reflection from these satellites with a ground-based telescope. For telescopes in the northern hemisphere, glint season occurs 2-4 weeks prior to the Spring equinox and 2-4 weeks after the Fall equinox. The selected GEO satellites will be observed before and after local midnight in order to measure their polarization and spectral signatures prior to, during, and after the glint.

I. Slitless Spectroscopy

The spectral method involves data processing through a MATLAB routine written in large part by previous USAFA cadets and faculty [6, 9]. We first rotate the spectral image because the grating is not perfectly aligned to the focal plane array's vertical axis, thus resulting in a spectrum that is slightly tilted. We then locate the zero order signature and clip the image to a 15 pixel wide sub-image centered on the satellite's first order spectrum. This allows us to measure the intensity across the spectrum. At this point, the spectrum is in pixel space, but can be converted to wavelength using a linear conversion. This conversion was determined in previous years using stars with known emission spectra, such as Wolf-Rayet stars, or stars with clear absorption lines such as Alhena and Vega.

Because the emission or absorption spectra of these stars are known, the pixel locations can be converted to wavelength by:

$$\lambda = 1.646 * P + 5.752, \tag{4}$$

Where $\boldsymbol{\lambda}$ is the wavelength in nanometers and P is the pixel location [6, 9].

In addition to performing the pixel to wavelength conversion, images where star trails and spectra contaminate our satellite signatures must also be removed (see Fig. 4). We do this in two steps with the first step automated and the second step manual. The first step is to determine the wavelength associated with the peak intensity value of a given satellite spectra. We then filter the images by only retaining those where the "peak" wavelength falls between 550 nm and 650 nm ($550\text{nm} < \lambda_{peak} < 650\text{nm}$). This range corresponds to a blackbody temperature between 5,269K and

Copyright © 2020 Advanced Maui Optical and Space Surveillance Technologies Conference (AMOS) – www.amostech.com

4,458K and consistent with previous measurements [6]. Although the sun's blackbody temperature is 5,778K corresponding to a wavelength of 502nm, we feel this first automated step removes any image with clear star contamination. For the second step, we manually view each remaining image and remove those that still show some star contamination. The amount of star trails appearing in the images varies depending on the time of year and amount of background stars in the field of view. After converting pixel to wavelength and removing star trails, the spectra of glinting satellites can be analyzed.

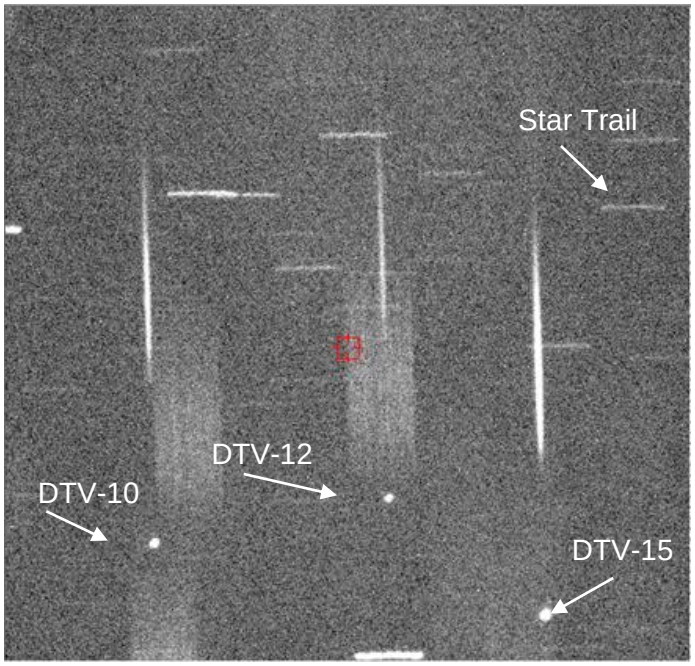

Fig. 4. Sample image of satellites DTV-10, 12, and 15 and their spectra. DTV-12 and DTV-15 spectra are influenced by stars below and above the zero order and are excluded from analysis.

II. Polarimetry

The polarimetry analysis uses commercial software and cadet-developed code to calculate polarization characteristics, including Stokes parameters, for the incident light. First a master dark is subtracted from all satellite images to remove thermal noise. Then the images are processed using a commercial application called Mira Pro. Mira Pro's aperture photometry tool determines the signal count for each satellite in a given image.

Copyright © 2020 Advanced Maui Optical and Space Surveillance Technologies Conference (AMOS) – www.amostech.com

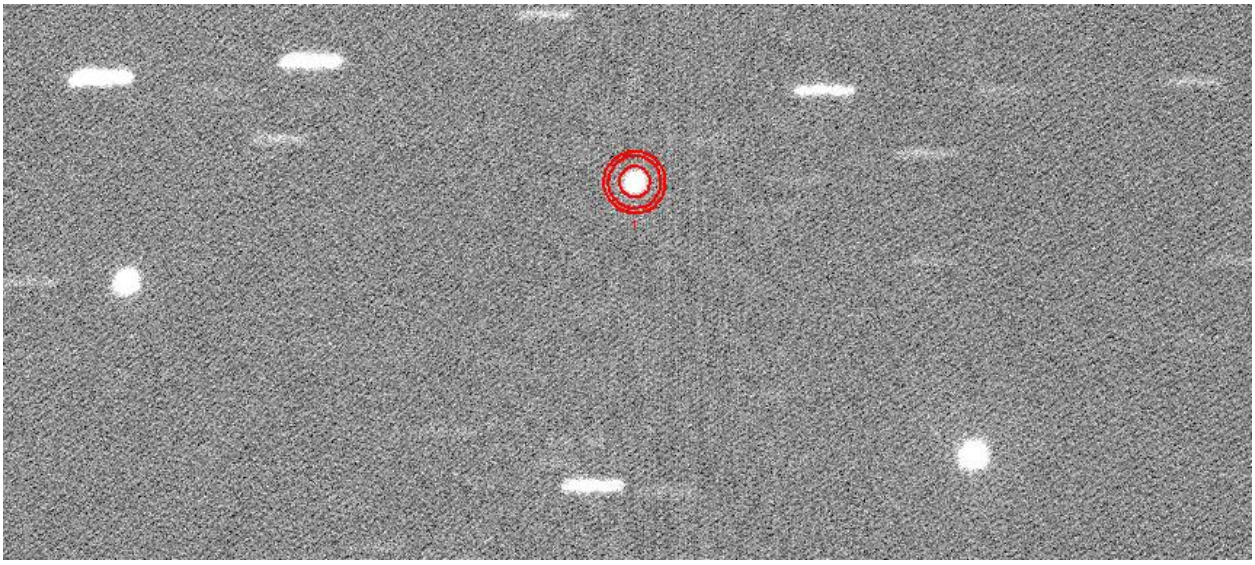

Fig. 5. Sample image of satellites DTV-10, DTV-12, and DTV-15 (from left to right) with Mira Pro aperture photometry markings. The counts within the red concentric circles around DTV-12 are measured for each image in the time series.

Aperture photometry measures the amount of light inside a designated aperture about a central point, in this case the target satellite. Two additional concentric circles about the satellite create an annulus; this measures background counts and is subtracted from the total raw counts, as shown in Fig. 5. Every count measurement was divided by exposure time to yield the equivalent counts per second. Finally, these measured intensities were converted into Stokes parameters using the *W* matrix conversion given in Eq (2). As in the spectroscopic analysis, all images corrupted by star trails within the chosen aperture around the satellite were removed. The degree of linear polarization (DOLP), a percentage measurement that describes the amount of linear polarization in light, was calculated for each satellite. The DOLP can be calculated from the first three Stokes parameters using the relation:

$$DOLP = \frac{\sqrt{{S_1}^2 + {S_2}^2}}{S_0} \tag{5}$$

5. RESULTS

We observed 5 clusters of 14 geosynchronous communication satellites on six different nights in the month of March 2020. These satellites were chosen based on past observations during a similar time of year. The table below outlines the satellites observed and whether or not they glinted.

Copyright © 2020 Advanced Maui Optical and Space Surveillance Technologies Conference (AMOS) – www.amostech.com

Table 1. Dates satellites were observed, name of the satellite, and glint presence.

DATE	SATELLITE	GLINT
03/03/2020	DTV-10	NO
	DTV-12	**NO**
	DTV-15	**GLINT**
03/04/2020	ANIK-F2	NO
	WB-1	**GLINT**
03/05/2020	AMC-15	NO
	SES-11	NO
03/10/2020	ANIK-F2	NO
	WB-1	NO
03/11/2020	SPACEWAY-2	NO
	DTV-11	NO
	DTV-14	**GLINT**
03/12/2020	**SPACEWAY-3**	**GLINT**
	IS-30	NO
	GALAXY-3C	NO
	IS-31	NO

Four of the satellites produced visible glints which were approximately one order of magnitude brighter than the satellite's optical signature at the start of the night. Due to the geometry of the satellite, the ground-based telescope, and the Sun, however, we were never able to observe a full glint due to the satellite moving into Earth's shadow. As a result, our data do not show the time period after each glint, and much of the data captures only the beginning of the glint. We will present preliminary results from four glinting satellites and one non-glinting satellite.

I. DTV-12

The data from observations of DTV-12 is included in order to provide baseline data for a satellite which does not appear to glint. DTV-12 was observed on the same night as the glinting satellite DTV-15, and both satellites were viewed in the same frame. The spectral analysis will be discussed first; this analysis fully characterized the spectral signature of the satellites. Fig. 6 illustrates the spectra of DTV-12 from 0545 to 0645 on 3 March, 2020 Coordinated Universal Time (UTC). Images were captured at 13 second intervals throughout that time, and results are shown in a graph with three axes. The x-axis displays the UTC time, while the y-axis is the wavelengths from 400 nm to 1000 nm. The z-axis and colorbar correspond to counts per second, or the relative intensity of the satellite signature. The black trace at the top of the plot tracks the wavelength value corresponding to the highest counts per second in the spectrum for each image. Fig. 6(b) is a two-dimensional view of the plot on the left, looking down from the z-axis to the xy-plane in order to better visualize the black trace's location on the wavelength axis.

Copyright © 2020 Advanced Maui Optical and Space Surveillance Technologies Conference (AMOS) – www.amostech.com

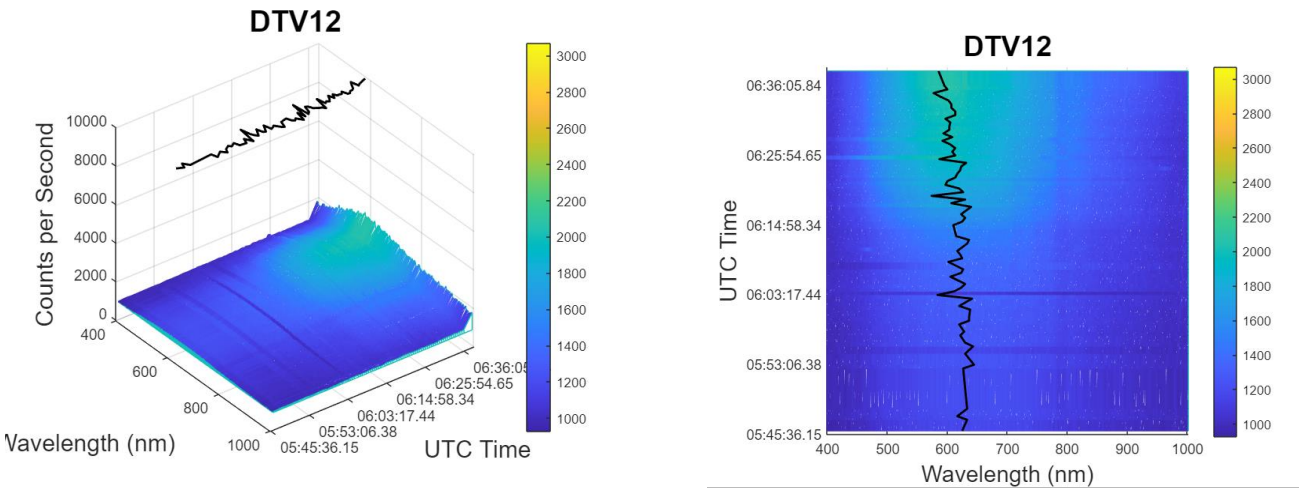

(a) (b)

Fig. 6. Plots of DTV-12 on 3 March, 2020. Fig. 6(a) is a view of the 3 dimensional plot, and Fig. 6(b) is a view from the top of the plot, looking onto the xy-plane.

For this non-glinting satellite, counts per second show a small increase toward the end of the observation period; this increase is not as significant as that of the glinting satellites. Additionally, Fig. 6 (b) shows that the wavelength at peak intensity remains constant over time, on average. The average wavelength at peak intensity is 615 ± 17 nm. Using Wien's displacement law, this wavelength corresponds to a reflectance temperature of 4,709 ± 128K. As a comparison, the sun's temperature is 5,778K.

As discussed in the caption for Fig. 3, linear polarization measurements are taken just before (P_0, P_{90}) and after (P_{135}, P_{45}) a spectral measurement. So although they are not simultaneous measurements, we can associate a group of measurements (P_0, P_{90}, DG, P_{135}, P_{45}) in a near-simultaneous fashion. Fig. 7(a) shows a plot of the Stokes parameters (S_0, S_1, and S_2) calculated from images of DTV-12 on 3 March 2020 from 0545 to 0645 UTC. Four images, one per polarization filter, were captured approximately every 13 seconds. The parameter S_0 (black trace) is plotted over time in black against the right vertical axis in units of counts per second. The other two measured Stokes parameters,, S_1 (green trace) and S_2 (red trace), are plotted in green and red against the left vertical axis, normalized to S_0. Fig. 7(b) shows the plot of the corresponding DOLP for DTV-12, normalized on a scale from 0 to 1.

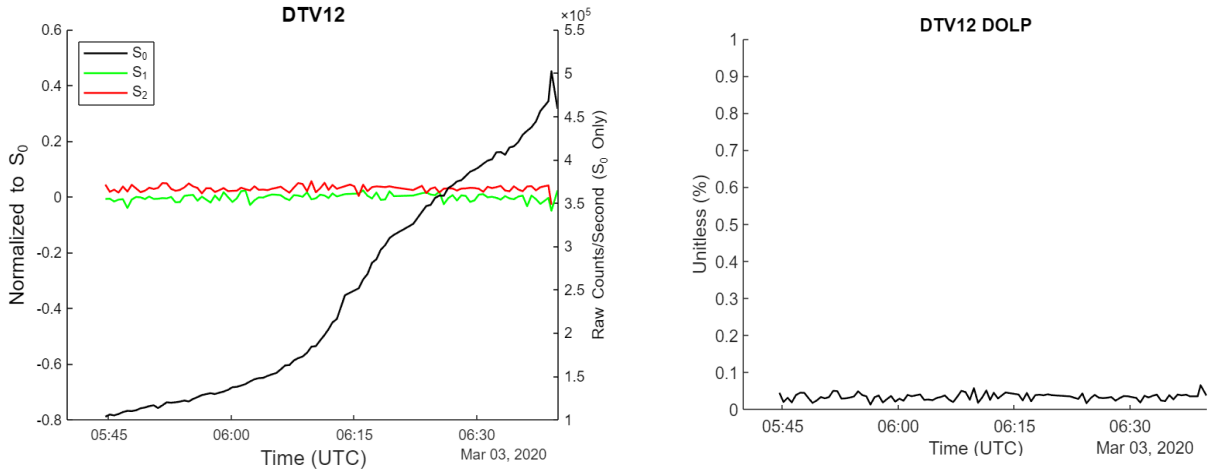

Copyright © 2020 Advanced Maui Optical and Space Surveillance Technologies Conference (AMOS) – www.amostech.com

(a) (b)

Fig. 7. Plots of polarization data collected from images of DTV-12 on 3 March, 2020. Fig. 7(a) is a plot of the Stokes parameters S_0 (against the right vertical axis) and S_1 and S_2 (against the left vertical axis), and Fig. 7(b) is a plot of the DOLP versus time.

As the total intensity (S_0)of DTV-12 increases by a factor of five throughout the observational period, the the S_1 and S_2 parameters remain fairly consistent with S_1 predominately negative (90° or horizontal) and S_2 predominately positive (45°). At approximately 0615 and 0622 however, S_0 shows pronounced dips resulting in no apparent effect to S_1, but with obvious and opposite spikes to S_2. This is also seen in the plot of DOLP, which in general shows rather low linear polarization (3-5%) except for those two times. Those two events are associated with some aspect of the satellite's surface that for some reason increases the polarization in the 45° and 135° directions, but has minimal effect on the 0° and 90° directions. These observations of the non- ginting DTV-12 serve somewhat as a baseline in order to compare the following glinting satellites.

II. DTV-15

Fig. 8 shows spectral data of DTV-15, observed from 0545 to 0645, 3 March, 2020 UTC, with images captured at 13 second intervals. This satellite was observed on the same night as the non-glinting satellite DTV-12. The format of Fig. 8 is the same as Fig.7, but with a red line in Fig. 8(b) representing the beginning of glint.

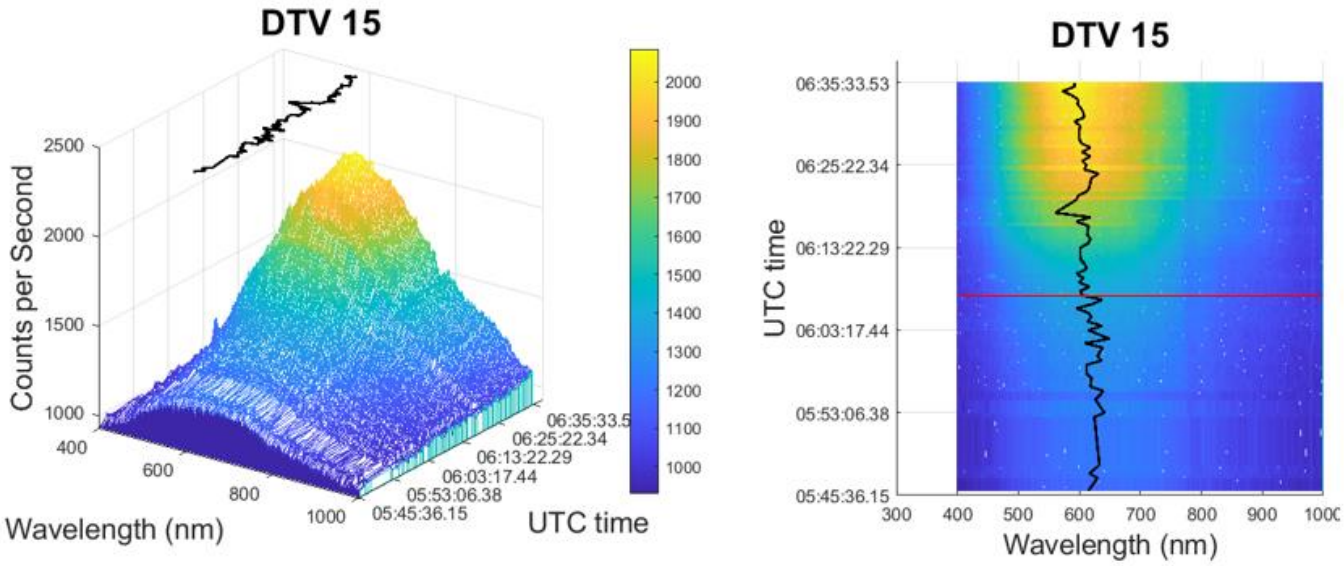

(a) (b)

Fig. 8. Plots of DTV-15 on 3 March, 2020. Fig. 8(a) is a view of the 3 dimensional plot, and Fig. 8(b) is a view from the top of the plot, looking onto the xy-plane. The red line in fig. 8(b) indicates the beginning of glint.

The peak wavelength was calculated for the glint time period; where glint begins when counts per second reached 15% of the maximum counts per second, as determined by previous spectral research [6]. The average wavelength at peak intensity during the glint period was 604 ± 12.6 nm. Using Wien's displacement law, this wavelength corresponds to a reflectance temperature of 4798 ± 99 K. Before glint, the average peak wavelength was 624 ± 13.7 nm, corresponding to a temperature of 4644 ± 102K. It is important to note that the wavelength at peak intensity for DTV-15 during glint is smaller than the wavelength before glint, in addition to being smaller than the wavelength of the baseline satellite, DTV-12. The corresponding temperature increased slightly during glint, and is accordingly smaller than the temperature of the non glinting satellite.

Copyright © 2020 Advanced Maui Optical and Space Surveillance Technologies Conference (AMOS) – www.amostech.com

The polarization signature of DTV-15 was also observed near simultaneously with its spectral signature. Fig. 9(a) shows a plot of the Stokes parameters (S_0, S_1, and S_2) calculated from images of DTV-15 on 3 March 2020 from 0545 to 0645 UTC.

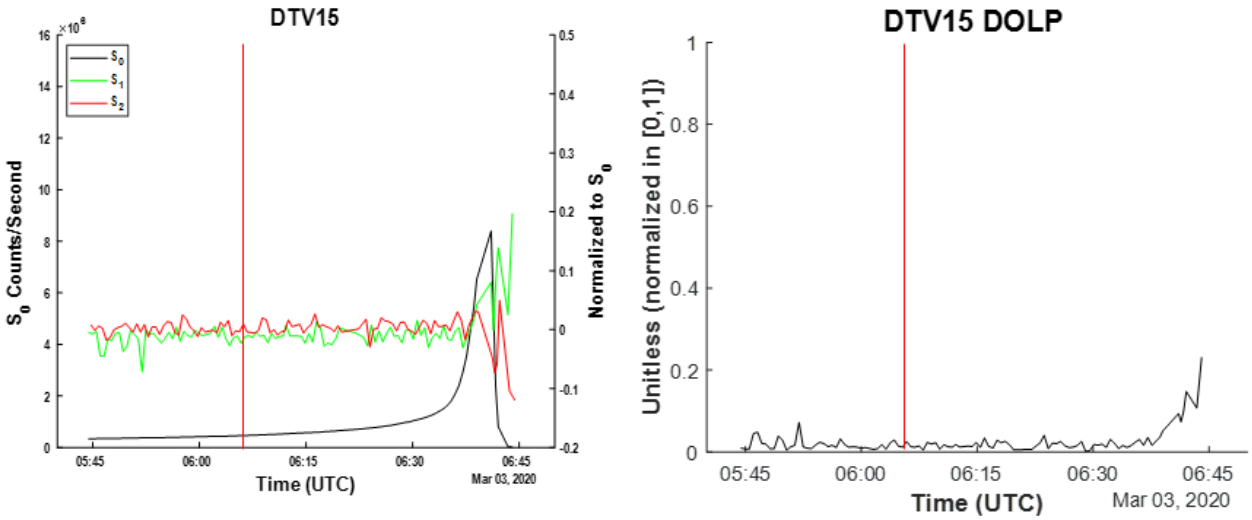

(a) (b)

Fig. 9. Plots of polarization data collected from images of DTV-15 on 3 March 2020. Fig. 9(a) is a plot of the Stokes parameters S_0 (against the left vertical axis) and S_1 and S_2 (against the right vertical axis), and Fig. 9(b) is a plot of the DOLP versus time. The red lines mark the beginning of glint.

The glint can be observed in Fig. 9(a) as a spike in the value of S_0, the total intensity, beginning around 0636 UTC. At the peak of the observed glint, the number of counts per second increased by over an order of magnitude compared to pre-glint levels. The polarization signatures of DTV-15, similar to DTV-12, shows a predominately negative S_1 (green trace) and a predominately positive S_2 (red trace). However, the values of S_1 and S_2 cross over and diverge at ~0636 UTC, when S_0 starts to increase dramatically, with S_1 increasing compared to its pre-glint value and S_2 decreasing. The DOLP also increases slightly during the glint period, to a maximum of about 0.25. The intensity of light sharply decreases around the end of the observation period because DTV-15 went into shadow at 0645 UTC.

III. Wildblue-1

Fig. 10 shows spectral data of Wildblue-1, observed from 0515 to 0712, 4 March, 2020 UTC, with images captured at 13 second intervals. These plots are in the same format as figs. 6 and 8.

Copyright © 2020 Advanced Maui Optical and Space Surveillance Technologies Conference (AMOS) – www.amostech.com

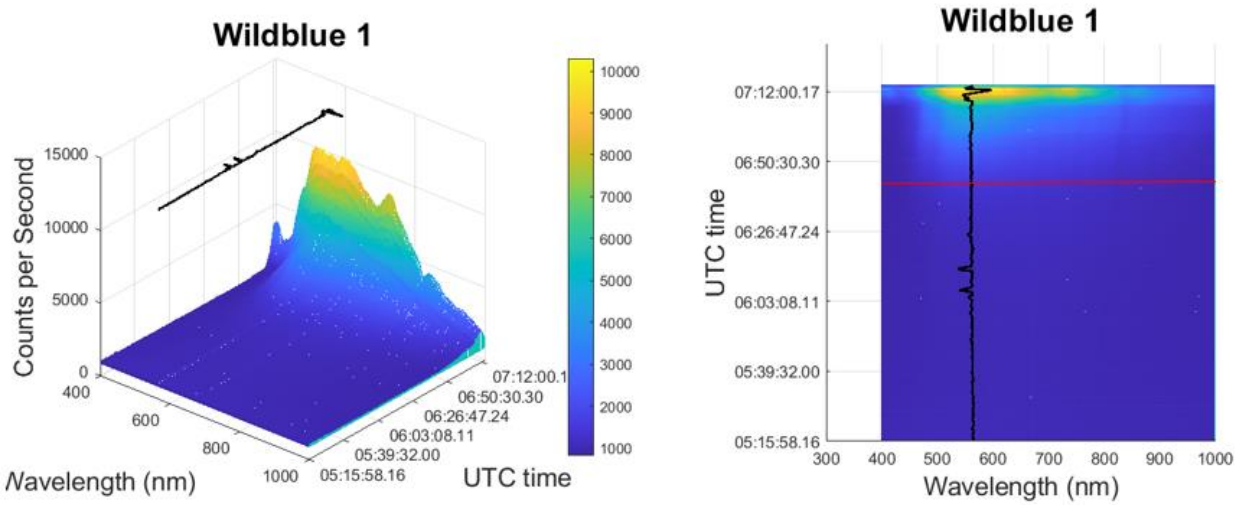

(a) (b)

Fig. 10. Plots of Wildblue-1 spectra collected 0515 to 0712, 4 March, 2020 UTC. Fig. 10(a) is a view of the 3 dimensional plot, and Fig. 10(b) is a view from the top of the plot, looking onto the xy-plane. The red line in fig. 10(b) indicates the beginning of glint.

During glint, the wavelength for the average peak intensity of Wildblue-1 was 560.6 ± 5.9 nm with a corresponding temperature of 5,170 ± 54K. Before glint, the peak wavelength was 561.9 ± 1.0 nm, with temperature 5,158 ± 9K. Toward the end of the glint, the spectrum of this satellite displayed an increase in intensity between 320 and 372 nm, or the UVA range. The other three satellites included in this analysis did not display an increase in intensity in this wavelength range. This could correspond to a unique material property on the satellite. Furthermore, this feature is unique to our data and has not been observed before; this observation, as compared to satellite properties, will be studied more in future work.

Fig. 11 shows plots of the Stokes parameters and DOLP calculated from images of Wildblue-1 on 4 Mar, 2020. This satellite was observed on 4 March, 2020 from 0515 to 0712 UTC. The plots are in the same format and on the same scale as those in figs. 8 and 10 and these images were also captured at 13 second intervals.

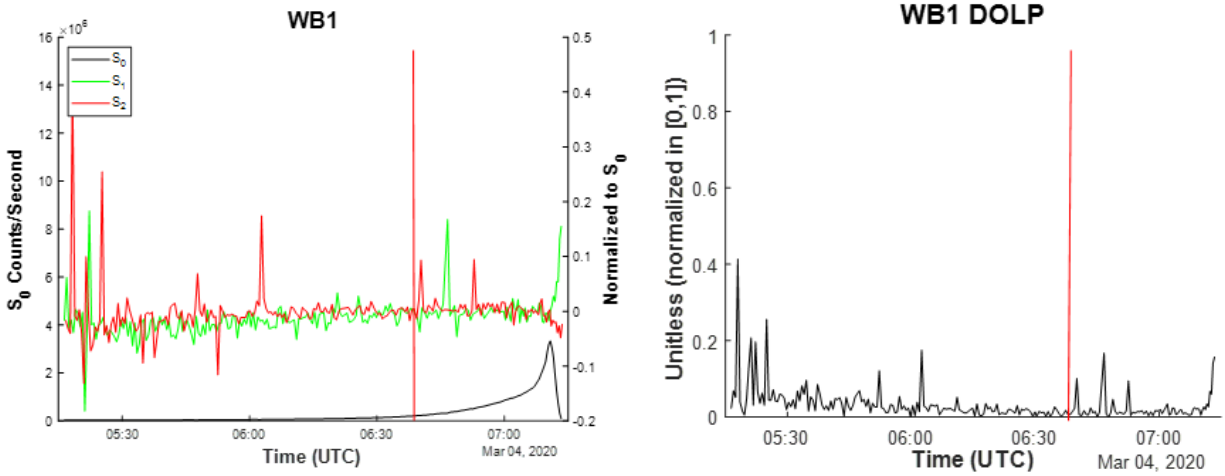

Copyright © 2020 Advanced Maui Optical and Space Surveillance Technologies Conference (AMOS) – www.amostech.com

(a) (b)

Fig. 11. Plots of polarization data collected from images Wildblue-1 on 4 March, 2020. Fig. 11(a) is a plot of the Stokes parameters S_0 (against the left vertical axis) and S_0 and S_0 (against the right vertical axis), and Fig. 11(b) is a plot of the DOLP versus time. The red lines mark the beginning of glint.

This glint was the smallest of the four we observed in terms of the spike in total light intensity, but still resulted in an increase in total intensity of an order of magnitude compared to pre-glint conditions. The satellite passed into shadow shortly after the total intensity started to spike. A divergence in the values of S_1 and S_2 and a slight increase in DOLP can be observed shortly before the satellite passed into shadow at 0712 UTC. The divergence in Stokes parameters and increase in DOLP occurred near simultaneously with the spectral anomaly in the UVA range.

IV. DTV 14

Fig. 12 shows spectral data of DTV-14, observed on 11 March 2020 from 0458 to 0614 UTC, with images captured continuously at 13 second intervals.

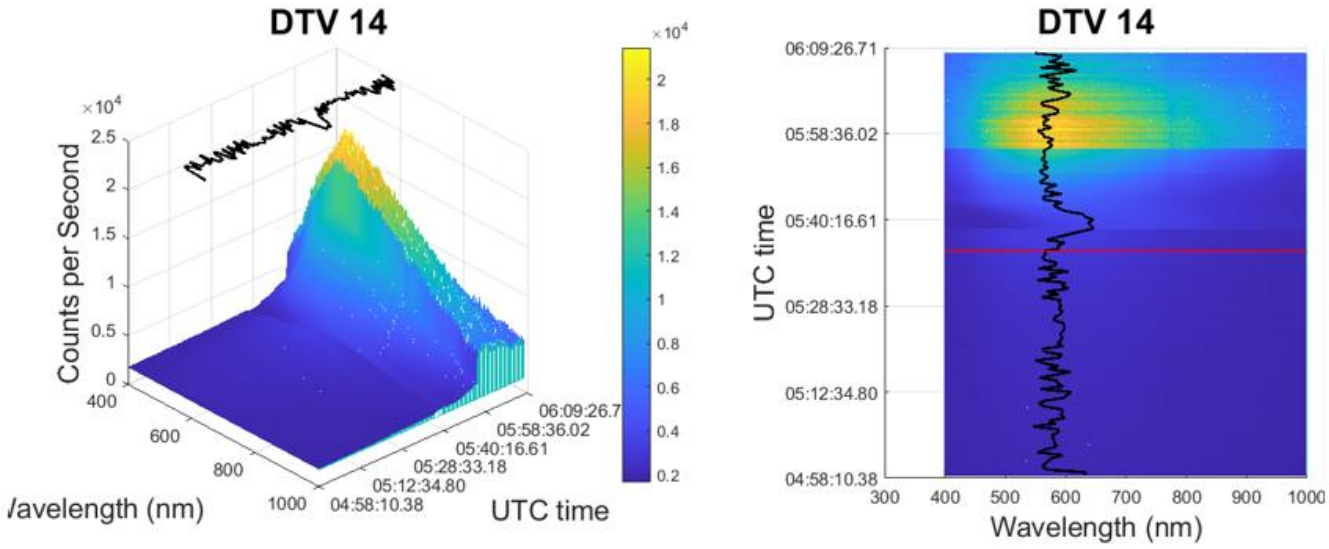

(a) (b)

Fig. 12. Plots of DTV-14 on 11 March, 2020. Fig. 12(a) is a view of the 3 dimensional plot, and Fig. 12(b) is a view from the top of the plot, looking onto the xy-axis. The red line in fig. 12(b) indicates the beginning of glint.

The average wavelength at peak intensity during glint is 576 ± 16.5 nm, and the corresponding temperature is 5,031 ± 143K. The average wavelength before glint is 585 ± 20.9 nm, with a temperature of 4,953 ± 177K. There was no obvious cause for the peak in wavelength seen just after glint begins, at approximately 0540 UTC. This will be evaluated further in future work.

Fig. 13 shows plots of the Stokes parameters and DOLP calculated from images of DTV-14 on 11 March, 2020 from 0458 to 0614 UTC. The plots are in the same format as the other polarimetry analysis plots and the images used were also captured at 13 second intervals.

Copyright © 2020 Advanced Maui Optical and Space Surveillance Technologies Conference (AMOS) – www.amostech.com

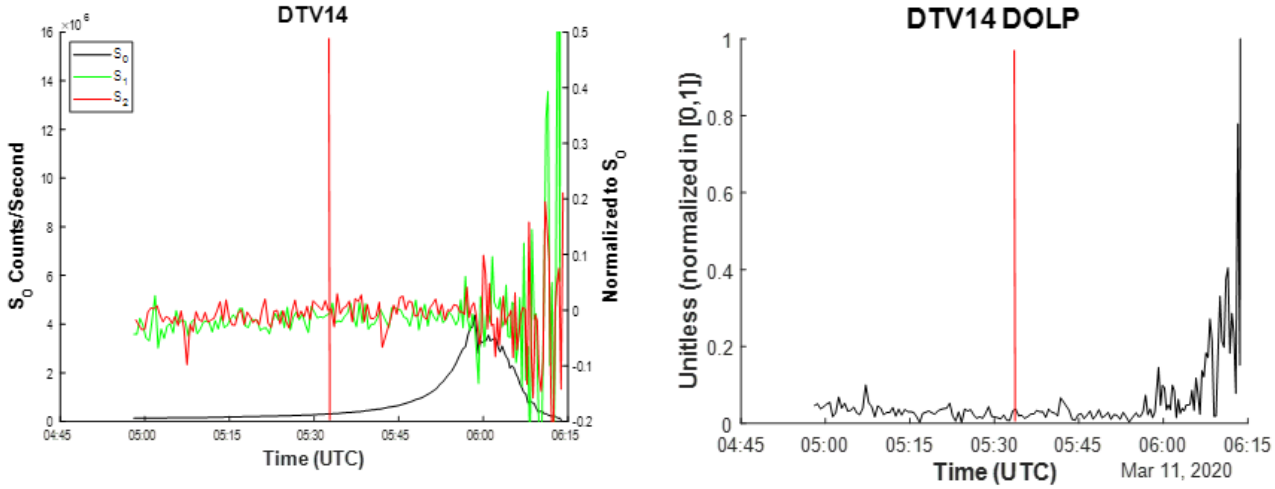

(a) (b)

Fig. 13. Plots of polarization data collected from images of DTV-14 on 11 March, 2020. Fig. 13(a) is a plot of the Stokes parameters S_0 (against the left vertical axis) and S_0 and S_0 (against the right vertical axis), and Fig. 13(b) is a plot of the DOLP versus time. The red lines indicate the beginning of glint.

This glint resulted in a smaller increase in total intensity compared to that of DTV-15. However, there was still an increase in total intensity of about an order of magnitude during the glint compared to pre-glint conditions. This corresponded to a significant increase in DOLP throughout the glint period, peaking right before the satellite entered shadow at around 0615 UTC.

V. Spaceway 3

Fig. 14 displays spectral data for Spaceway-3, which was observed on 12 March 2020 from 0451 to 0557 UTC at 13 second intervals.

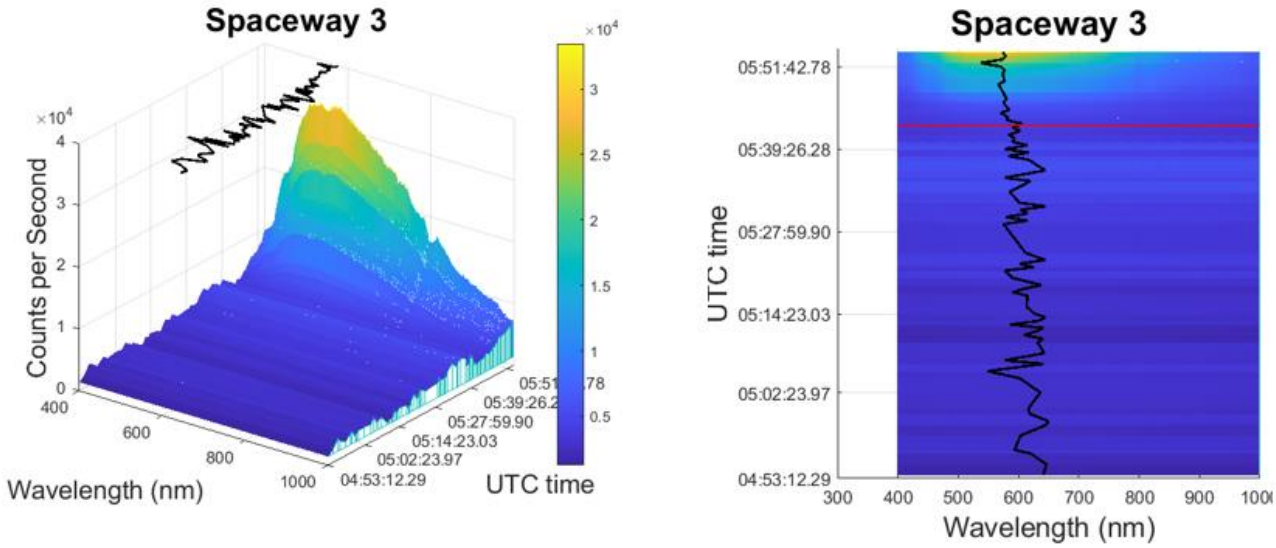

Copyright © 2020 Advanced Maui Optical and Space Surveillance Technologies Conference (AMOS) – www.amostech.com

(a) (b)

Fig. 14. Plots of Spaceway-3 on 12 March, 2020. Fig. 14(a) is a view of the 3 dimensional plot, and Fig. 14(b) is a view from the top of the plot, looking onto the xy-plane. The red line in Fig. 14(b) indicates the beginning of glint.

This satellite glinted for a short period of time before entering shadow, but counts per second increased by an order of magnitude during glint. The average wavelength at peak intensity was 566.4 ± 15.4 nm. The temperature was 5,116 ± 139K. The average peak wavelength before glint is 606.3 ± 25.6 nm, with a temperature of 4,780 ± 201K.

Fig. 15 shows plots of the Stokes parameters and DOLP calculated from images of Spaceway-3 (SW-3) on 12 March, 2020. This satellite was observed from 0451 to 0557 UTC. The plots are in the same format as the other polarimetry analysis plots and the images used were also captured at 13 second intervals.

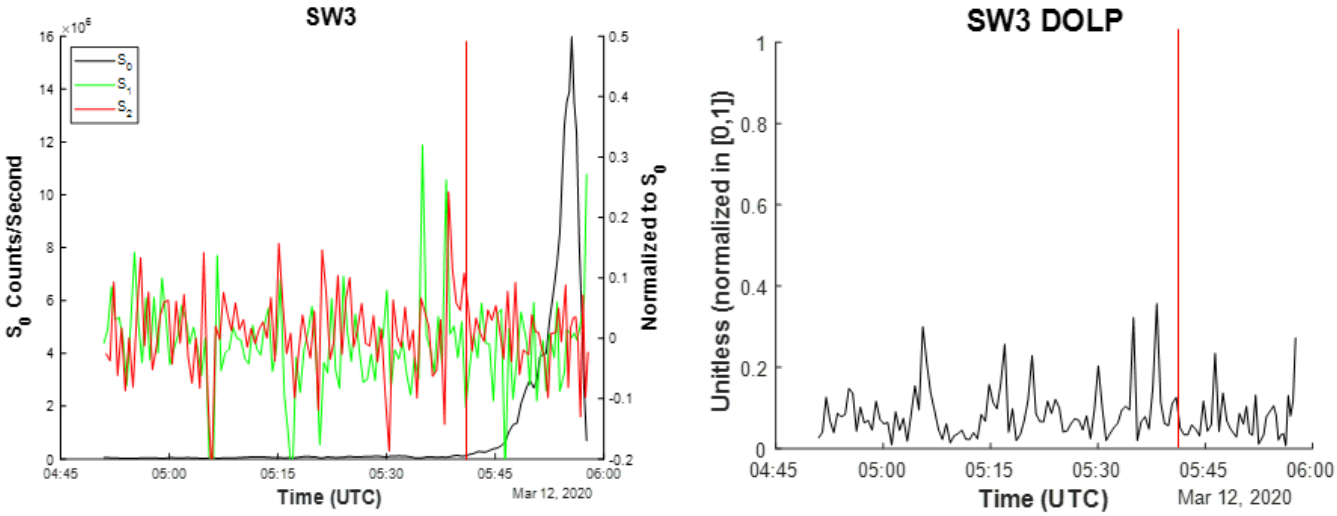

(a) (b)

Fig. 15. Plots of polarization data collected from images of Spaceway-3 on 12 March 2020. Fig.15(a) is a plot of the Stokes parameters S_0 (against the left vertical axis) and S_0 and S_0 (against the right vertical axis), and Fig. 15(b) is a plot of the DOLP versus time. The red lines mark the beginning of glint.

These plots show a very pronounced glint, with total intensity increasing by over an order of magnitude during the glint before the satellite passed into shadow at around 0557 UTC. However, there was no clear trend in the DOLP during the glint as there was in Figs. 9 (b), 11(b), and 13(b). The stokes parameters S_1 and S_2 also do not display any visible trends.

6. CONCLUSIONS

We collected data on four glinting satellites and successfully processed this data in order to make comparisons between the two optical modes. Although each of the satellites moved into Earth's shadow shortly after the glint began, the observations still yielded useful data. Spectral data processing allowed us to determine the average wavelength at peak intensity and reflectance temperature for each satellite, and polarimetry yielded calculations for Stokes parameters and degree of linear polarization.

Copyright © 2020 Advanced Maui Optical and Space Surveillance Technologies Conference (AMOS) – www.amostech.com

When analyzing features of the polarization optical mode, S_1 and S_2 showed more variability during glint. For three of the glinting satellites, the DOLP began to increase when the satellite glinted. These characteristics were not visible for DTV-12, the non-glinting satellite included in this analysis. In the spectral mode, we were able to determine a correlation between wavelength at peak intensity during the glint compared with before the glint. When the satellite undergoes specular reflection, the sunlight reflected from the satellite should have very similar spectral properties to the Sun's spectrum. As a result, the wavelength at peak intensity during the glint should be close to the peak wavelength of the Sun's blackbody spectrum, or 550 nm. A shorter average wavelength during glint compared to before glint was observed consistently for the four satellites; the wavelength during glint was closer to the Sun's wavelength for each satellite. The wavelength during glint was also, on average, shorter than the wavelength for non-glinting satellite DTV-12. The wavelength before glint is longer perhaps because the reflected light is coming from more diffusive satellite surfaces present on the body of the satellite rather than the solar panels.

We also made comparisons between the two optical modes. Wildblue-1's spectrum displayed increased intensity in the 320-370 nm wavelength range as compared with the spectral signature before glint. This feature was not observed in any other satellite's spectral data. This signifies a reflection of photons in the UVA spectral range, which may be indicative of material properties of the satellite. When comparing this spectral data with the polarization data, there was a corresponding feature in Wildblue-1's polarization signature. The signature showed a divergence in S_1 and S_2 occurring in the same time period in which the spectrum was displaying an increased wavelength range. This is a correlation between the spectral and polarimetry data that can be further analyzed in order to understand satellite features and positioning.

7. FUTURE WORK

Our observations are preliminary and require further analysis. Future work should entail continued observations of satellite spectroscopic and polarimetry signature data. Similar to the analysis done on the 320-370 nm range of Wilblue-1, further work should also include looking for corresponding features in both optical modes. By finding correlations in both optical modes, this research should enable the ability to glean material properties and positioning data of the observed satellites, thus achieving the overall research goal of unresolved satellite characterization and enhancing Space Domain Awareness capabilities.

8. ACKNOWLEDGEMENTS

The authors would like to thank the Air Force Office of Scientific Research for supporting this research. Additionally, this paper is the result of a senior capstone project in the Department of Physics at the United States Air Force Academy. This paper has been cleared for public release. DISTRIBUTION STATEMENT A: Approved for public release: distribution unlimited. PA#: USAFA-DF-2020-308

Copyright © 2020 Advanced Maui Optical and Space Surveillance Technologies Conference (AMOS) – www.amostech.com

REFERENCES

[1] Joint Publication 3-14, "Space Operations,' 10 April 2018.

[2] D. Fulcoly, K. Kalamaroff, and F. Chun, "Determining Basic Satellite Shape from Photometric Light Curves," *Journal of Spacecraft and Rockets*, **49** (2012).

[3] D. Hall, K. Hamada, T. Kelecy, and P. Kervin, "Surface Material Characterization from Non-resolved Multi-band Optical Observations," *The 2012 AMOS Technical Conference Proceedings*, The Maui Economic Development Board, Inc., Kihei, Maui, HI, 200-209 (2012).

[4] K.J. Abercromby, K. Hamada, M. Guyote, J. Okada, and E. Barker, "Remote and Ground Truth Spectral Measurement Comparisons of FORMSAT III," *The 2007 AMOS Technical Conference Proceedings*, The Maui Economic Development Board, Inc., Kihei, Maui, HI, 379-388 (2007).

[5] D. Bédard, G. Wade, D. Monin, and R. Scott, "Spectrometric characterization of geostationary satellites," *Proceedings of the 2012 AMOS Technical Conference*, The Maui Economic Development Board, Inc., Kihei, Maui, HI (2012).

[6] A.N. Dunsmore, J.A. Key, R.M. Tucker, E.M. Weld, F.K. Chun, and R.D. Tippets, "Spectral Measurements of Geosynchronous Satellites During Glint Season," *J. Spacecraft and Rockets* **54**, 349-355 (2016).

[7] A. Speicher. "Identification of Geostationary Satellites Using Polarization Data from Unresolved Images", Ph.D. Thesis, University of Denver, 2015.

[8] M. Pirozzoli, L. Zimmerman, M. Korta, A.D. Scheppe, F.K. Chun, M.K. Plummer, C.N. Harris, and D.M. Strong, "Characterization of Unresolved Satellite Imagery Using Polarization Data," presented at the Annual American Astronomical Society Conference, Honolulu, HI, 2020 (unpublished).

[9] R.D. Tippets, S. Wakefield, S. Young, I. Ferguson, C. Earp-Pitkins, and F.K. Chun, "Slitless spectroscopy of geosynchronous satellites," *Optical Engineering* **54**, 104103 (2015). doi:10.1117/1.OE.54.10.104103

Copyright © 2020 Advanced Maui Optical and Space Surveillance Technologies Conference (AMOS) – www.amostech.com